Journal of Catalysis 371 (2019) 346–356

Contents lists available at ScienceDirect

Journal of Catalysis

journal homepage: www.elsevier.com/locate/jcat

Promotional effects of magnesia on catalytic performance of Pt/SiO_2 in hydrogenolysis of dibenzofuran

Jie Zhang [a], Chuang Li [a], Xiao Chen [a], Yujing Chen [a], Liyun Zhang [b], Bingsen Zhang [b], Changhai Liang [a,*]

[a] State Key Laboratory of Fine Chemicals, Laboratory of Advanced Materials and Catalytic Engineering, School of Chemical Engineering, Dalian University of Technology, Dalian 116023, China
[b] Shenyang National Laboratory for Materials Science, Institute of Metal Research, Chinese Academy of Sciences, Shenyang 110016, China

ARTICLE INFO

Article history:
Received 14 November 2018
Revised 17 January 2019
Accepted 15 February 2019

Keywords:
Dibenzofuran
Hydrogenolysis
Pt/SiO_2
Magnesia
Biphenyl

ABSTRACT

Developing mechanistic insights into the promotional effect of alkaline earth metal oxides in the hydrogenolysis of lignin-derived dibenzofuran (DBF) is key to rational design of high-performance catalysts for bio-oils upgrading. The promotional effect of MgO on Pt/SiO_2 catalyst for the hydrogenolysis of DBF has been investigated. Small amounts of MgO enriches the electron density of Pt surface and the Lewis acidity of support, leading to significant improvement of the reactivity with an excellent turnover frequency (TOF) of 1182 h^{-1} on $Pt/3MgO/SiO_2$ compared with 789 h^{-1} on Pt/SiO_2. The high selectivity for biphenyl depends on the combination of the acid-base properties. With the same moles of alkaline earth dopants, the activity of dopants decreased in the order: Mg > Ca > Sr > Ba, resulting from the decrease in Pt dispersion, and, decreasing linearly with decreasing electronegativity. Additionally, in 240 h stability test, $Pt/3MgO/SiO_2$ catalyst showed considerably stable activity and selectivity.

1. Introduction

Fossil-derived resources depletion and the associated environmental deterioration constantly draw the attention for their replacement by renewable resources. Dibenzofuran (DBF), an inexpensive and versatile oxygen-containing compound, widely exists in the nonconventional fuel liquids, such as coal tar, shale oil and bio-oil [1–4]. It may be used as the starting material for the production of liquid fuels [5–8] and some useful compounds [9,10] such as biphenyl (BP), *o*-phenylphenol (OPP) and other derivatives. BP has been considered as a key target molecule for its various applications as an organic intermediate, a precursor to cycloalkane based transportation fuels, and pesticide. Hydrogenolysis of DBF to BP represents a highly environmentally benign, sustainable and efficient route and the process can guide the removal of oxygen to increase volatility and thermal stability of bio-oil [11].

Recently, magnesia is widely used as the promoter for enhancing the activity of catalysts in many catalytic reactions, such as glucose isomerization [12], the hydrogenation of acetylene [13], hydrodesulfurization reaction [14,15], ethanol-to-butadiene process [16–18], and aldol condensation [19]. Numerous findings have proposed several reasons for the role as promoter of MgO for improving the activity of catalysts in term of fine dispersion of active metals, the acid-base properties of the supports or electronic effect. A large number of positive results showed that the addition of alkaline metal oxides could change the physical structure of the support, which altered the amount of the active components [20,21]. However, it was also proposed [14] that the effect on the support was to change the acid properties of the already formed surface, but practically the structure of the supports remained unaffected. Others proposed that the promotional effects of the alkaline dopants on the catalytic activity of mesoporous Co_3O_4 for 4-nitrophenol reduction were due to the electronic changes rather than structural changes in the catalysts [22]. The literature [15] argued that the addition of a small amount of MgO could change the morphology of active sites such as the stacking of MoS_2, decrease the weak Brønsted acidity of the supports, and increase the electron density, thus improving the intrinsic hydrogenation activity. Nevertheless, the introduction of MgO could also improve the concentration of weak Lewis acidic sites [20] due to the presence of additional Lewis sites - ions of Mg^{2+} [14]. On the other hand, the enhanced activity was also attributed to the promoted hydrogen-spillover effect by the moderate acidic sites due to the generation of new species with addition of MgO [13]. However, few studies have reported on the promotional effect of MgO on the catalysts in hydrodeoxygenation (HDO) reaction and less of a clear mechanistic insight has been revealed into the promotional effect of alkaline earth metal oxides in HDO reaction.

* Corresponding author.
E-mail address: changhai@dlut.edu.cn (C. Liang).
URL: http://www.amce.dlut.edu.cn (C. Liang).

https://doi.org/10.1016/j.jcat.2019.02.017
0021-9517/

In our previous work [10], the target product in the hydrogenolysis of dibenzofuran was o-phenylphenol by the reasonable design of catalyst. It is found the basic sites promoted the formation of o-phenylphenol. Herein, our goal is to extend this knowledge by modifying different Mg loadings on Pt/SiO_2 in an attempt to improve the production of biphenyl. MgO, as the catalyst promoter, was found to increase activity and BP selectivity of Pt/SiO_2 catalyst for the hydrogenolysis of DBF. Characterization techniques such as XRD, IR, CO-IR, low temperature N_2 sorption, NH_3-TPD, CO_2-TPD, Py-IR, TEM, SEM, were used to study the structural property, electronic effect and the surface acid-base property of catalysts. Moreover, the role of other alkaline earth metal (Ca, Sr, Ba) oxides on the activity of Pt/SiO_2 catalyst was also investigated. Finally, the reaction mechanistic understanding for the hydrogenolysis of DBF to biphenyl over $Pt/xMgO/SiO_2$ catalysts has been proposed. This work demonstrates for the first time the importance of employing a suitable addition of MgO in the rational development of Pt-based catalysts for the hydrogenolysis of DBF. The experimental results presented can provide a rational and useful guidance for designing Pt-based hydrogenolysis catalysts.

2. Experimental

2.1. Materials

Silica ($348\ m^2\ g^{-1}$) was purchased from Aladdin Chemical Reagent Co and used as support after the calcination at 400 °C for 2 h under Air. Magnesium acetate ($Mg(CH_3COO)_2{\cdot}4H_2O$, ≥99.0%), calcium nitrate ($Ca(NO_3)_2{\cdot}4H_2O$, ≥99.0%), strontium nitrate ($Sr(NO_3)_2$, ≥99.5%), barium nitrate ($Ba(NO_3)_2$, ≥99.5%), and chloroplatinic acid ($H_2PtCl_6{\cdot}6H_2O$, Pt basis 99.9%) were purchased from Sinopharm Chemical Reagent Co. Methanol (CH_3OH, 99.8%) and n-decane ($C_{10}H_{22}$, 98%) were obtained from Tianjin Kermel Chemical Reagent Co. Dibenzofuran ($C_{12}H_8O$, ≥98.0%), 2-methylpiperidine ($C_6H_{13}N$, 99.0%) and n-dodecane ($C_{12}H_{26}$, 99.0%) were obtained from Aladdin Chemical Reagent Co. All of the materials were analytical reagent grade and utilized without further purification.

2.2. Catalyst preparation

2.2.1. Preparation of $Pt/xMgO/SiO_2$ catalysts

Commercial SiO_2 was impregnated by the wetness impregnation method with an aqueous $Mg(CH_3COO)_2$ solution in order to prepare supports with different Mg loadings (1, 3, 6, 9 wt%). The obtained supports, denoted as $xMgO/SiO_2$, where x is the weight percentage of Mg (x = 0, 1, 3, 6, 9), were dried overnight at 100 °C, and finally calcined at 500 °C for 4 h under Ar/O_2 ($40/20\ mL\ min^{-1}$) flow.

The as-synthesized supports were used to prepare Pt catalysts by successive wetness impregnation method using $H_2PtCl_6{\cdot}6H_2O$ as Pt precursor, methanol as the solvent, with a targeted Pt content of 0.5 wt%. The Pt samples were dried at 80 °C overnight and then reduced at 400 °C for 2 h under a H_2 flow of $40\ mL\ min^{-1}$ before catalytic performance test and the characterization of catalysts. The obtained catalysts are designated as $Pt/xMgO/SiO_2$.

2.2.2. Preparation of $Pt/MO/SiO_2$ (M = Ca, Sr, Ba) catalysts

Other catalysts modified by alkaline earth metal oxides ($Pt/MO/SiO_2$, M = Ca, Sr, Ba) were obtained by a sequential impregnation method as above. The Pt and alkaline earth metal loadings of these catalysts were consistent with the moles of $Pt/3MgO/SiO_2$, respectively. All actual atomic ratio of M/Pt are approximately 50:1 as shown in Table 1.

2.2.3. Preparation of reference catalysts

For comparison, the reference $Pt\text{-}3MgO/SiO_2$-co catalyst was prepared by co-impregnation of the appropriate amount of aqueous $Mg(CH_3COO)_2$ and Pt precursor solution, remaining 3 wt% Mg. The following treatment of obtained sample was the same as above. In the binary catalyst, the two functional components of Pt/SiO_2 catalyst and MgO were combined just by physical mixing (Pt/SiO_2 + MgO).

2.3. Support characterization

2.3.1. Nitrogen adsorption

The textural properties of the supports were determined using the nitrogen adsorption–desorption isotherms at −196 °C using a Quantachrome Autosorb IQ automated sorption system. The specific surface area was calculated using the Brunauer–Emmett–Teller method at a relative partial pressure of 0.05–0.3. The total pore volume and pore size distribution were measured by the adsorption curve using the Barre–Joyner–Halenda model at a relative partial pressure of 0.95. Prior to the measurement, the samples were degassed under vacuum at 200 °C for 8 h.

2.3.2. X-ray diffraction

X-ray diffraction (XRD) analysis of the supports was performed on a Rigaku D/MAX-RB instrument using a Cu Kα monochromatized radiation source in the 2θ range of 5–90° with a scan speed of $10°\ min^{-1}$, operated at 40 kV and 100 mA.

2.3.3. Temperature-programmed desorption

The acidity and basicity of the supports were measured by Temperature-programmed desorption (TPD) of NH_3 and CO_2, respectively, using the CHEMBET-3000 instrument with a thermal conductivity detector (TCD). Typically, 100 mg sample was pressed, crushed, and placed in U-shaped glass tube, heated to 500 °C ($10\ °C\ min^{-1}$) in He, and this temperature was kept for 60 min. Then the sample was cooled down to 120 °C. The ammonia adsorption was conducted for 40 min under a $20\ mL\ min^{-1}$ flow of 10 vol% NH_3 in He gas mixture. The physically adsorbed ammonia was removed under helium flow at 120 °C for 60 min, and the TPD was measured by linearly increasing the cell temperature from 120 °C to 500 °C at a heating rate of $10\ °C\ min^{-1}$ under a $20\ mL\ min^{-1}$ flow of He. The amount of desorbed ammonia was monitored and quantified by measuring the areas of the desorption profiles. Similarly, the basicity of the sample was determined by CO_2-TPD, a method analogous to that described above.

2.3.4. FT-IR spectroscopy of pyridine adsorption

Fourier transform infrared spectra (FT-IR) experiments using pyridine as the probe molecule, on a Bruker Equinox 55 spectrometer equipped with a DTGS detector, were conducted in the IR cell at 150 °C, 300 °C and 450 °C, using 10 mg sample pellets. The supports were evacuated at 450 °C for 30 min and then cooled to room temperature, followed by the record of a background at a resolution of $4\ cm^{-1}$. After that, the samples were saturated with pyridine flow for another 20 min. Then the IR spectra were taken at room temperature after evacuation for 30 min at 150 °C to remove physically adsorbed and residual pyridine. The adsorption of pyridine at 300 °C and 450 °C were similar to that at 150 °C.

2.3.5. Infrared attenuated total reflection spectrum

Fourier transform infrared attenuated total reflection spectra (ATR-FTIR), using a Thermo Fisher iN10 spectrometer equipped with a liquid-nitrogen-cooled MCT detector, were recorded within the spectral range of 650–4000 cm^{-1} with a resolution of $4\ cm^{-1}$ and 16 scans for signal accumulation.

Table 1
Properties of alkaline earth metal oxide promoted supports and catalysts.

Samples	S[a] (m^2/g)	V_p[b] (cm^3/g)	d_p[c] (nm)	Pt loading[d] (wt.%)	M loading[d] (wt.%)	(M/Pt) atomic ratio (1 0 [2])	Reaction rate[e] ($\mu mol \cdot g_{cat}^{-1} \cdot s^{-1}$)	CO uptake (μmol/g)	TOF[f] (h^{-1})	Pt dispersion (%)
Pt/SiO_2	348	1.04	12.0	0.49	–		2.89	6.87	789	27
$Pt/1MgO/SiO_2$	305	0.91	11.8	0.50	1.03	0.16	3.45	6.70	961	26
$Pt/3MgO/SiO_2$	288	0.84	11.6	0.56	3.53	0.51	6.00	7.17	1182	28
$Pt/6MgO/SiO_2$	258	0.75	11.6	0.43	6.66	1.24	3.22	5.68	1148	26
$Pt/9MgO/SiO_2$	219	0.62	11.4	0.47	9.74	1.66	2.76	5.83	1017	22
$Pt/CaO/SiO_2$	264	0.78	11.8	0.37	3.46	0.45	2.23	3.80	1159	15
$Pt/SrO/SiO_2$	181	0.55	12.0	0.42	9.62	0.51	1.07	1.68	726	6
$Pt/BaO/SiO_2$	120	0.36	12.6	0.32	10.57	0.47	0.33	0.88	681	5
$Pt\text{-}3MgO/SiO_2$-co	–	–	–	0.48	3.35	0.56	1.86	–	–	–
Pt/SiO_2 + MgO	–	–	–	0.52	3.21	0.50	2.87	–	–	–

[a,b,c] Support properties determined by BET.
[d] Measured by ICP-AES (M = Mg, Ca, Sr or Ba).
[e] The reaction rate $= \frac{\text{converted moles of dibenzofuran}}{\text{the weight of catalyst} * \text{contact time}}$, at low conversion.
[f] Obtained from CO chemisorption at 30 °C. Supposed CO/Pt = 1.

2.4. Catalyst characterization

2.4.1. High resolution transmission electron microscopy

The interface of the metal-support in $Pt/3MgO/SiO_2$ catalyst was characterized by a high resolution transmission electron microscopy (HRTEM) with a Tecnai G2 F20 (FEI) instrument operating at 200 kV. Before the measurements, the sample was ultrasonically dispersed in ethanol and the suspension formed was deposited onto a copper grid.

2.4.2. Scanning electron microscopy

A field–emission scanning electron microscopy (FEI Nova Nano SEM 450) was used to characterize the homogeneity of dispersion of Pt and MgO on SiO_2. SEM-EDX analyses were operated at 200 kV and performed with a Tecnai F20 apparatus, equipped with an energy-dispersive X-ray (EDX) detector.

2.4.3. FT-IR spectroscopy of CO adsorption

Fourier transform infrared spectra (FT-IR) of CO adsorption, collected on a Bruker Equinox 55 spectrometer equipped with a DTGS detector, were used as a standard method to investigate the electronic states of the Pt surface. A varying dilution of the samples in KBr (1:20–1:2) was used to account for the different Mg loadings. Prior to adsorption, the already reduced samples at 400 °C were placed into the reaction chamber and reduced in flowing H_2 (10% in Ar) at 300 °C for 60 min again to avoid the oxidation of Air. After cooling to 25 °C, the samples were purged in flowing He for 30 min followed by adsorption of CO (10% in He) at a flow rate of 20 mL min^{-1}. An adsorption time of 40 min was found to be sufficient to observe the saturation coverage. Then removal of the gas phase CO with molecular pump was complete until the spectra were unchanged, and the spectra were collected by coaddition of 500 scans at a scanner velocity of 10 kHz and a resolution of 4 cm^{-1}.

2.4.4. Elemental analysis (ICP-AES)

The metal contents of the catalysts were measured by inductively coupled plasma atomic emission spectroscopy (ICP-AES) on a Perkin-Elmer Optima 2000 DV device.

2.4.5. CO chemisorption

A chemisorb analyzer using CO pulse adsorption on CHEMBET-3000 was used to measure the accessibility of metal surface sites at 30 °C. Prior to measurement, the *ex situ* reduced catalysts were activated *in situ* in H_2 at 400 °C for 1 h and purged in flowing He followed by adsorption of CO (10% in He) when the furnace was cooled to 30 °C. CO adsorption was considered to be completed after three successive peaks showing the same peak areas. A stoichiometry of CO/metal = 1 was taken to calculate the number of metal active sites. Hence, the turnover frequency (TOF) and dispersion of the Pt active sites of the catalyst can be evaluated.

2.5. Activity measurements

Typically, the hydrogenolysis of DBF was performed at 400 °C and 1.0 MPa total pressure in a continuous-flow fixed-bed reactor over 80 mg catalyst diluted with 5.0 mL 60–80 mesh quartz sands. Prior to catalytic tests, the as-prepared catalysts were pretreated *in situ* under 40 mL min^{-1} flow of H_2 at 1.0 MPa and 400 °C for 1 h. Catalytic tests were conducted until the steady state was reached. The liquid reactants consisted of 2.0 wt% DBF, 1.0 wt% *n*-dodecane (as internal standard) and 97.0 wt% *n*-decane (as solvent). The reaction products after being condensed in a cold trap were collected and analyzed off-line by an Agilent gas chromatograph 7890A equipped with flame ionization detector and a 0.5 μm × 0.32 mm × 30 m FFAP capillary column. Product identifications were conducted on an Agilent 7890B with 5977A MSD and a 0.25 μm × 0.25 mm × 30 m HP-5 capillary column.

The $Pt/3MgO/SiO_2$ catalyst was selected for a long-run test. The long-run test was carried out in fixed-bed reactor and performed in the hydrogenolysis of DBF until steady state was reached. The products were obtained after six hours each time. And to investigate the effect of acidic sites of catalysts, the effect of 0.5 wt% 2-methylpiperidine (2-MPP) added to the reactant during the hydrogenolysis of DBF was studied and the reaction process is the same as the above procedure.

The conversion (X) of DBF was calculated by the equation

$$X = (n_0 - n_{DBF})/n_0 \times 100\% \quad (1)$$

where n_0 and n_{DBF} are the moles of DBF in the feed and product, respectively.

The selectivity (S_i) for each product (i) was calculated by the equation

$$S_i = n_i / \sum n_i \times 100\% \quad (2)$$

where n_i is the moles of i product molecule and $\sum n_i$ are the total moles of products. The carbon balance of products was 100% ± 5%.

Contact time (τ) was calculated from the formula

$$\tau = W/F \quad (3)$$

where W denotes the catalyst weight and F denotes the total weight flow rate of the reactant.

3. Results and discussion

3.1. Physical texture of samples

xMgO/SiO_2 supports were synthesized by an impregnation with commercial amorphous SiO_2 and then calcined at 500 °C. In the XRD patterns of all catalysts (Fig. S1), no crystalline minor phases was observed, even with higher loading of Mg. It indicates that Pt and the added Mg are randomly deposited on the surface. However, it is not determined whether the active Pt is dispersed on the SiO_2 surface or the interface of MgO and SiO_2 for the addition of Pt to MgO/SiO_2 supports.

The N_2 adsorption-desorption isotherms of all samples are very similar, as shown in Fig. S2. And the detailed results are revealed in Table 1. All isotherms are type IV isotherms and display the H1 hysteresis loops, which are typical characteristics for mesoporous materials. BET analysis of the promoter-modified supports shows that incorporation of alkaline earth metal oxides on the SiO_2 leads to a significant reduction on both the specific surface area and pore volume as increasing amount of Mg or ionic radius (Ca, Sr, Ba), compared to the pure SiO_2 (as listed in Table 1), revealing that alkaline earth metal oxides could block the mesopores. Nevertheless, pore diameter has no appreciable variation in all promoter-modified catalysts, which rules out the fact that pore size is not one of the possible promotional effect.

Table 1 summarizes the Pt dispersions measured by CO chemisorption and TOFs for different catalysts. The addition of large excesses of MgO did not have obvious impact on the Pt dispersion, which was approximately 26%, until 6 wt% Mg loading was reached. However, compared with the catalysts modified by various alkaline earth metal oxides with equal mole, it was observed that the Pt dispersion follows the order: Mg > Ca > Sr > Ba, which could be explained by the decrease in specific surface area due to the increased ionic radius. Considering the slight difference of Pt dispersions over MgO/SiO_2 mixing oxides supported Pt catalysts, it is not considered as one reason for the enhanced performance of Pt/xMgO/SiO_2 catalysts.

3.2. Acid–base properties of the xMgO/SiO_2 supports

To investigate the acid-base properties of the xMgO/SiO_2 supports, the interaction of NH_3 and CO_2 with the xMgO/SiO_2 supports were studied by temperature-programmed desorption experiments, in combination with ATR-FTIR spectroscopy and IR spectroscopy of adsorbed pyridine.

The ATR-FTIR spectra of xMgO/SiO_2 supports are plotted in Fig. S3. Three absorption bands at 1057 cm^{-1}, 973 cm^{-1} and 796 cm^{-1} can be assigned to the Si—O—Si stretching mode [23]. The band at 680 cm^{-1} can be attributed to the Mg—O stretching vibration [17]. MgO addition broadens the band at 1057 cm^{-1} and weakens the strength of the bands at 973 cm^{-1} and 796 cm^{-1} compared to the pure SiO_2, accompanied with the blue-shift of Si—O—Si bands at 1057 cm^{-1} and 796 cm^{-1} to a lower wavenumber (1033 cm^{-1} and 790 cm^{-1}), indicative of the strengthened interaction between MgO and SiO_2, preferentially generating a Si—O—Mg bond [24] and maybe suggesting the existence of additional magnesium silicate phase [16]. The small blue shift suggests the existence of Si—O—Mg linkages, since Si has higher electronegativity than Mg, and similarly that was also found in the TiO_2/SiO_2 catalysts [25]. The band at 1636 cm^{-1} can be assigned to the bending vibration of the water molecules. The broad band at 3400 cm^{-1} belongs to the stretching vibrations of the hydroxyl groups of water physically adsorbed on the surface [26,27]. Indeed, the surface silanol groups can be in the presence of the band at 3745 cm^{-1} [27], which could be due to the weak interaction with adsorbed water on the silica surface. However, they were not found due to the coverage of water physically adsorbed on the surface.

Acidity and basicity of xMgO/SiO_2 were characterized from temperature-programmed desorption of adsorbed NH_3 and CO_2, and the calculated results are listed in Table 2. The MgO addition leads to an increase and then stabilization in the basicity of the supports, and that was in agreement with the fact that the presence of alkaline/alkaline earth ions could result in a marked increase of the basic properties of the catalysts [28,29]. However, the amount and strength of acidic sites also significantly increased when adding MgO to SiO_2. The amounts of NH_3 and CO_2 desorbed from 3MgO/SiO_2 approximately increase to 250.2 and 18.2 μmol/g, respectively, compared with that of pure SiO_2 (32.0 and 2.5 μmol/g). It is suggested that the modification by MgO significantly increases the number of acidic and basic sites of the supports, nevertheless, the number of acidic sites far exceed that of basic sites.

The IR spectra of pyridine adsorbed on a series of xMgO/SiO_2 supports at 150 °C, plotted in Fig. S4, contained both bands of pyridine coordinated to Lewis acidic sites (1446 cm^{-1}) and bands of pyridinium cations formed by reaction of pyridine with Brønsted acidic sites (1547 cm^{-1}). The values of Lewis acidic sites listed in Table 2 show that, with the addition of MgO, the Lewis acidic sites dramatically increased initially and then slowly decreased for further MgO addition due to the appearance of Mg^{2+} [14,19] and mainly the existence of additional magnesium silicate phases [16] as confirmed by ATR-FTIR. The density of Lewis acidic sites was much higher than that of Brønsted acidic sites (Table 2), whereas the disparity between them diminished with the addition of MgO. Furthermore, the latter was null after desorption at 450 °C (Fig. 1b), indicating that the strength of Brønsted acidic sites is weaker than that of the Lewis acidic sites.

3.3. FT-IR spectra of CO adsorption

The acid-base properties of the support could strongly influence the catalytic performance of the supported metal nanoparticles. One reason is attributed to the interaction between the acidic or basic supports and the active metals, inducing electronic effects required for the catalytic reactions [13,15].

Table 2
The acid-base properties of the xMgO/SiO_2 supports.

Samples	Amount of acidic sites (μmol/g)			Amount of basic sites (μmol/g)
	Lewis sites	Brønsted sites	Total sites	Total sites
SiO_2	31.5	0.5	32.0	2.5
1MgO/SiO_2	111.1	0.8	111.9	9.5
3MgO/SiO_2	240.4	9.8	250.2	18.2
6MgO/SiO_2	210.7	14.6	225.4	42.2
9MgO/SiO_2	191.4	25.4	216.8	39.3
MgO[a]	11.2	0.1	11.3	45.7

Note: a is bulk phase prepared by the thermal decomposition of $Mg(CH_3COO)_2$ as a reference.

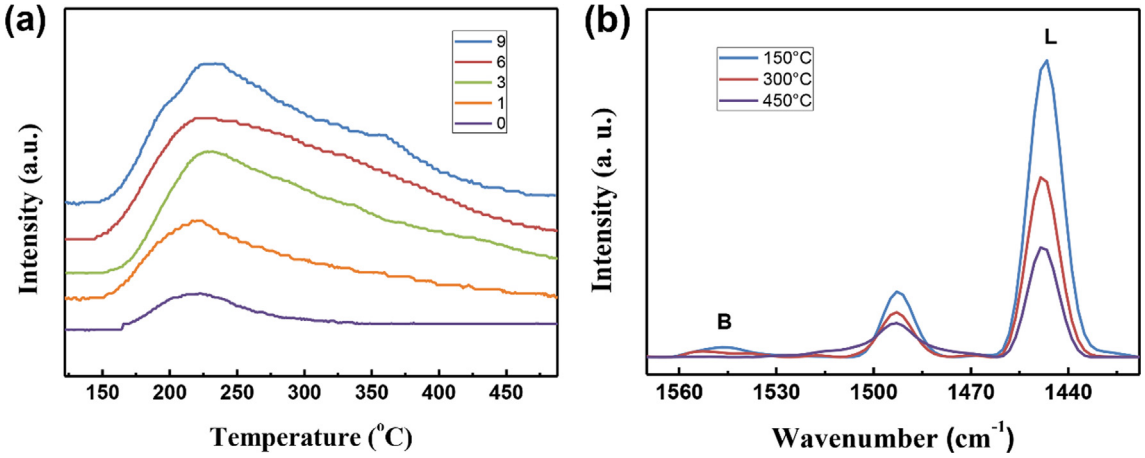

Fig. 1. (a) NH_3-TPD profiles of the $xMgO/SiO_2$ (x = 0, 1, 3, 6, 9), and (b) IR spectra of pyridine adsorbed on $3MgO/SiO_2$ support at 150, 300 and 450 °C.

The IR bands after *in-situ* reduction of $Pt/xMgO/SiO_2$ catalysts and CO adsorption at 25 °C have been used to characterize the surface electronic properties of supported Pt nanoparticles. The CO-FTIR spectra were integrated and results are summarized in Fig. 2. Two main bands were observed in the spectra: a broad, strong band appeared in 2000–2120 cm^{-1} that are assigned to a linear CO, and another broad and less intensive signal at about 1850 cm^{-1} that corresponds to bridged CO [30–33]. CO adsorption on Mg^{2+} cation is expected to yield one or more additional band at 2157–2200 cm^{-1} approximately, in which as the number of O^{2-} anions (n) coordinated to Mg^{2+} decreases, the signal of CO shifts to higher wavenumbers ($\upsilon_{n=4}$ = 2157 cm^{-1}, $\upsilon_{n=3}$ = 2200 cm^{-1}) [19]. However, no such band can be clearly identified in our case due to the weaker intensities of the bands.

The shift in the CO band position is often interpreted as the evidence of the changes in the electronic properties of supported metals [31,34]. The exact position of the absorption bands depends on the electronic changes [35], particle size [36], and surface coverage [37]. Since the Pt dispersion of the $Pt/xMgO/SiO_2$ catalysts does not vary with the Mg content (Table 1), the shifts in the band position probably reflect the changes in the surface electronic properties of catalysts. Besides, the intensity ratio of bridged to linear (B/L) bonded CO is also a critical parameter and a direct measurement of the energy difference between the interacting d-orbitals of active surface metal sites and the $2\pi^*$ orbital of CO [34], which reveals the surface electron density of the supported Pt particles.

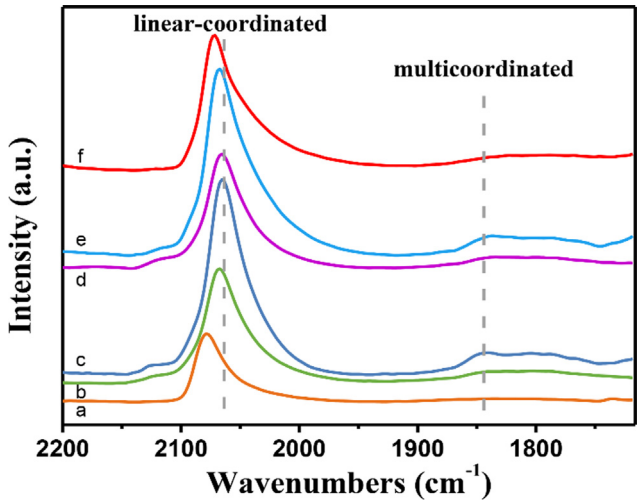

Fig. 2. IR spectra of CO adsorbed on $Pt/xMgO/SiO_2$ after *in-situ* reduction at 300 °C in flowing H_2 (a-e: 0, 1, 3, 6, 9 wt% Mg, and f Pt-$3MgO/SiO_2$-co).

Variation of the band position and the areas of linear and bridged CO measured are listed in Table 3, demonstrating that electron transfer occurs. The wavenumber shifted from 2078 to 2064 cm^{-1} in the $Pt/xMgO/SiO_2$ samples with increasing the Mg content to 3 wt%, but the band position slightly shifted to higher wavenumbers with higher Mg content, indicating that the electron density of Pt in $Pt/3MgO/SiO_2$ strikingly increases. Similar trends have also been observed for the $PtFe/SiO_2$ system and such a shift is associated with an increase in the electron density on Pt [30], which in turn increases the extent of the back donation to the CO $2\pi^*$ orbitals [35]. The intensity of the signals corresponding to linear adsorption decreased, while that of the bridged CO band increased with increasing the Mg content in the supports. The increasing B/L ratio with increasing the Mg content in the support also indicates an increase of the electron density. It is in agreement with previous studies on Pt supported on K-modified Al_2O_3 [34] and Pt supported on Cs_2O-modified Al_2O_3 [31], which is typical for Pt on a base doped support. However, the inverse trend was observed when the Mg content was 3 wt% with the maximum B/L value. This indicates that there are more isolated Pt sites separated by MgO on the surface of $Pt/xMgO/SiO_2$ catalysts (x > 3) [13]. The change of electronic structure could be due to the change in the surface acidic/basic sites of supports, and the basic sites of support increase the electron density of Pt [13]. The IR bands of adsorbed CO shifted to lower wavenumbers and the B/L ratio increased by the modification of basic promoter, resulting in an increase in electron charge of oxygen atoms of the support and hence an increase in electron density on the supported Pt particles [38,39]. Besides, the shift of the CO band position to lower wavenumbers indicates a lower oxidation state of Pt [40], and it is also confirmed that the reduction of oxidation state of active metal could be influenced by the alkaline promoter [41]. The FTIR results of chemisorbed CO are a strong indication that the electronic structure of the catalytically active surface metal sites is influenced by the modification of MgO.

3.4. Transmission electron microscopy

Fig. 3 shows TEM images of the $Pt/3MgO/SiO_2$ catalyst after hydrogen reduction at 400 °C, clearly revealing that the metallic nanoparticles were uniformly dispersed on the silica support. HRTEM observations on $Pt/3MgO/SiO_2$ revealed the presence of separate MgO and Pt NPs over SiO_2, and the active Pt surrounded by MgO (Fig. 3a), thereby indicating that individual MgO and Pt

Table 3
The results of CO-IR over various catalysts.

Sample	Location of Linear band (cm^{-1})	Integrated area of the band (%)		Bridged and linear area ratio (B/L)
		Linear CO	Bridged CO	
Pt/SiO_2	2078	90.61	9.39	0.10
$Pt/1MgO/SiO_2$	2068	87.72	12.28	0.13
$Pt/3MgO/SiO_2$	2064	87.49	12.51	0.14
$Pt/6MgO/SiO_2$	2065	88.10	11.90	0.13
$Pt/9MgO/SiO_2$	2068	88.92	11.08	0.12
$Pt\text{-}3MgO/SiO_2\text{-}co$	2072	93.72	6.28	0.07

NPs are present on the SiO_2 surface and Pt locates at the boundary between MgO and SiO_2 support. Positively, the magnified region (Fig. 3b) confirmed that Pt nanoparticles are in direct contact with the magnesia substrate and may preferentially migrate onto the interface between SiO_2 and MgO by the reduction. The d-spacing values of 0.197 and 0.227 nm correspond to the (2 0 0) and (1 1 1) plane of Pt. On the other hand, the MgO exposes more (2 0 0) plane with interlayer spacing of 0.210 nm. The HRTEM results indicated that the MgO in close contact with the Pt species stabilizes the dispersion of Pt on silica. STEM results (Fig. 3c and d) showed that metallic NPs were small and uniformly dispersed on the support. To figure out the intrinsic structures of the $Pt/3MgO/SiO_2$ catalyst in a large region, STEM-mapping measurement was performed (Fig. 4) and the results clearly showed that the MgO and Pt were only partly overlapping in the tested region, indicating the active Pt is surrounded by MgO. It is the evidence for the existence of Pt-magnesia-silica interfaces. The TEM results may provide useful information in the catalytic performance (discussed in below).

In order to calculate the particle sizes of Pt, the TEM and corresponding particle size distributions of all catalysts were shown in Fig. S5. The obtained average particle sizes of $Pt/xMgO/SiO_2$ catalysts were similar (~1.60 nm), indicating the similar Pt dispersion according to previous reports [42,43], which was in agreement

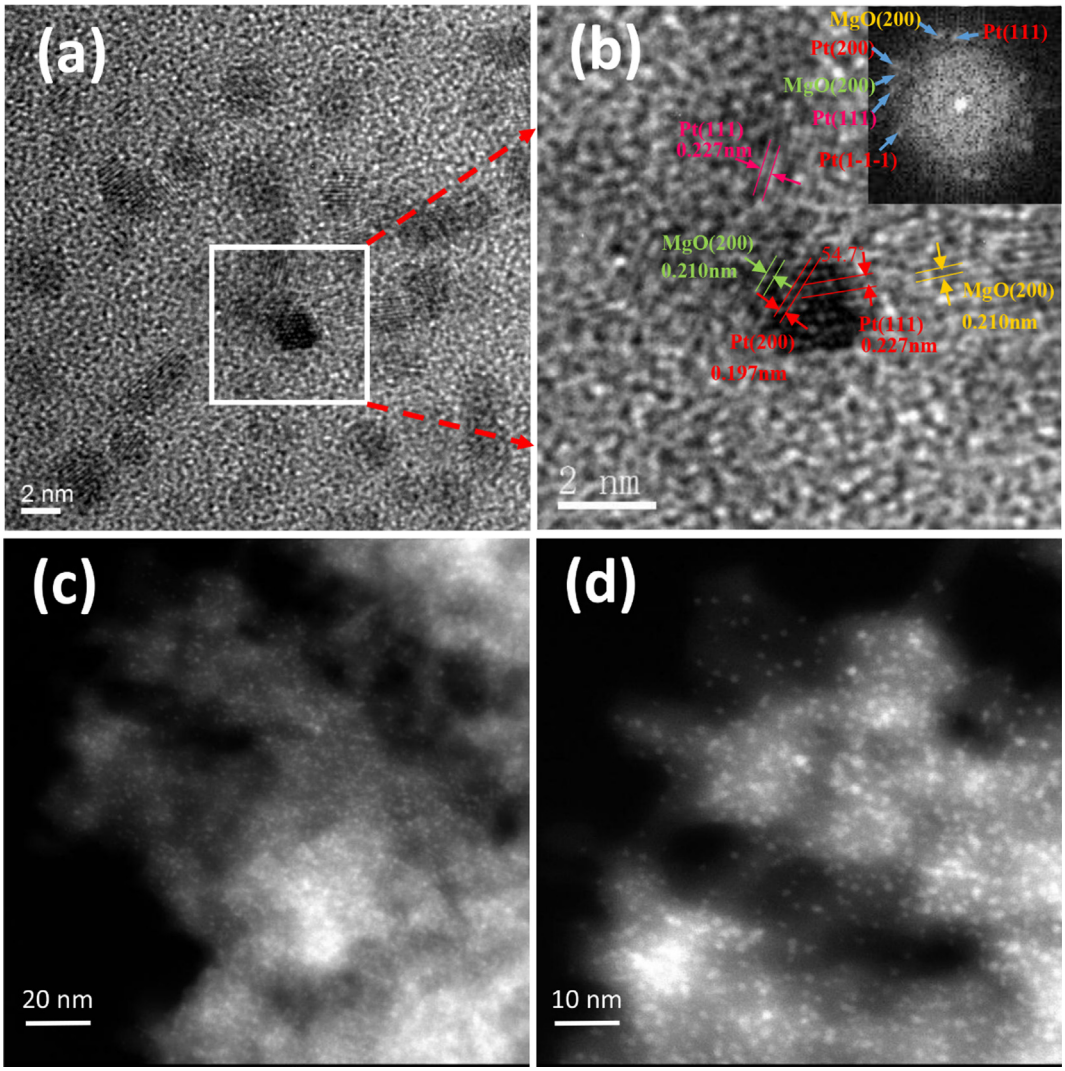

Fig. 3. HRTEM image (a, b) and STEM (c, d) of the representative $Pt/3MgO/SiO_2$ catalyst after reduction at 400 °C for 2 h.

with the results of CO chemisorption (Table 1). Besides, the average Pt particle sizes were increased in order of Pt/MgO/SiO_2 (1.56 nm) < Pt/CaO/SiO_2 (2.32 nm) < Pt/SrO/SiO_2 (2.67 nm) < Pt/BaO/SiO_2 (2.96 nm), with the decreased Pt dispersion (Table S3). Correspondingly, the Pt dispersion calculated from CO adsorption followed the same tendency (Table 1).

3.5. Scanning electron microscopy

In order to determine the elemental distribution, SEM-EDX analysis was performed and the images are shown in Fig. S6. The mapping images show that there is a good correspondence of Mg elemental map formed with the intensity of Si element, indicating the MgO uniformly distributed on the surface of SiO_2. And Mg loading is 3.43 wt%, which is of no obvious disparity with the result tested by ICP (3.53 wt%). However, Pt particles with low loading (0.5 wt%) were not detected.

3.6. Catalytic results of the hydrogenolysis of DBF

The hydrogenolysis of DBF was used to evaluate the catalytic behavior of Pt/xMgO/SiO_2 catalysts and the Pt/SiO_2 catalysts modified with various alkaline earth metal oxides. The hydrogenolysis products, such as *o*-phenylphenol (OPP), biphenyl (BP), cyclohexylbenzene (CHB), cyclopentylmethylbenzene (CPMB), cyclohexane (CH) and benzene (B) were determined by the GC–MS, as shown in Fig. 5. With increasing contact time, almost all were deoxygenated product. The major hydrogenolysis product was BP with the highest yield of 68% at contact time of 0.55 min with a conversion of 100%. As shown in Table 4, at contact time of 0.16 min, the BP selectivity enhanced dramatically from 42.7% (Pt/SiO_2) to 55.0% (Pt/1MgO/SiO_2) and then to the maximum of 63.2% (Pt/3MgO/SiO_2), followed by a decrease to 46.1% in pace with the gradual addition of MgO. Moreover, with the addition of MgO, CaO, SrO or BaO, respectively, the conversion sharply decreased and the selectivity toward OPP increased (see Table 5).

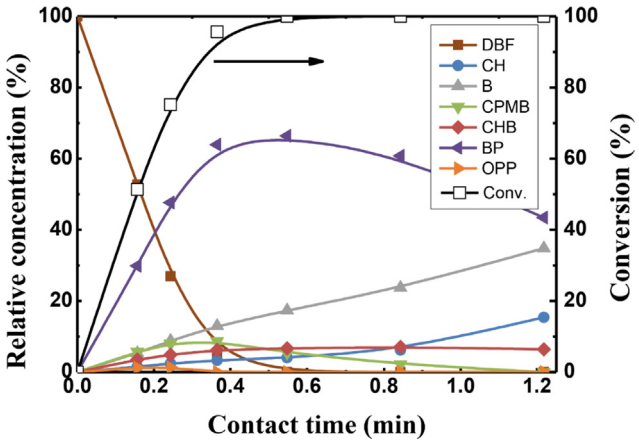

Fig. 5. Relative concentration and conversion of the hydrogenolysis of DBF over Pt/3MgO/SiO_2 as a function of contact time.

3.6.1. Catalytic performance: Volcano-type dependence on Mg loading

The activities of Pt/xMgO/SiO_2 catalysts in the hydrogenolysis are plotted in Fig. 6a. It is interesting to find out that activities vary with the Mg loadings in a volcano-shape manner, and the optimum catalyst is Pt/3MgO/SiO_2 sample. The conversion of the hydrogenolysis of DBF increased with the addition of Mg (3 wt%) and then dramatically decreased with further Mg addition. Meanwhile, the BP yield showed a similar trend with the highest yield obtained of 64%. This volcano-type dependency of reaction activities on Mg loadings was the same as the trend of the intrinsic activities (TOF) and reaction rate (Table 1). The promotional catalyst had the maximum activity at 3 wt% loading, and that is almost twice higher than that over Pt/SiO_2. It can be inferred that a fraction of MgO is beneficial for the hydrogenolysis of DBF. The possible reasons are shown in Fig. 6b and were discussed below.

The FTIR data for CO adsorption (Table 2) reveals a higher fraction of electron-rich and reduced Pt sites over the promoted catalysts. The acid-base properties of the supports have an important effect on the electron state of active sites [44,45]. As illustrated in the reports [31,46], basic sites participated in the catalytic process via increasing the electron density of Pt. The report [13] discussed the role of acidic and basic sites of PdAg/Mg-Ti catalysts in the hydrogenation of acetylene and found the increased Pd electronic density caused by the electron transfer from the basic sites. However, it is well known that the acidic sites could also directly promote the activation and then the cleavage of C—O bond [5,47,48]. Indeed, MgO addition results in the changes of physical-chemical structure of the supports and subsequently leads to specific acid-base properties of catalysts. It is speculated that the electronic perturbation of Pt could be attributed to the interaction between Pt and surface acidic/basic sites of MgO/SiO_2

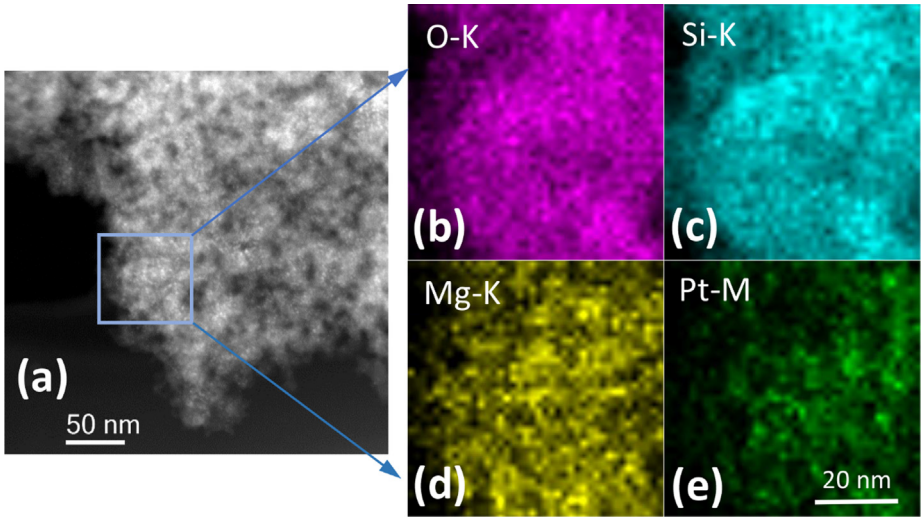

Fig. 4. (a) STEM of Pt/3MgO/SiO_2 revealing the EDS mapping region and (b–e) the EDS mapping of all kinds of elements (O, Si, Mg and Pt).

Table 4
Effect of catalyst on the DBF conversion and product selectivity.

Catalyst	Conversion (%)	Selectivity (%)					
		CH	B	CPMB	CHB	BP	OPP
Pt/SiO_2	26.6	0	6.5	3.5	5.1	42.7	42.2
$Pt/1MgO/SiO_2$	31.5	1.9	8.9	8.7	7.2	55.0	18.3
$Pt/3MgO/SiO_2$	51.4	3.2	11.3	12.1	7.5	63.2	2.7
$Pt/6MgO/SiO_2$	27.7	2.1	12.7	16.3	9.2	51.8	7.9
$Pt/9MgO/SiO_2$	22.0	1.6	18.7	13.1	8.1	46.1	12.4
$Pt/CaO/SiO_2$[a]	18.3	0.4	6.4	1.9	3.8	18.9	68.6
$Pt/SrO/SiO_2$[a]	12.4	0	8.7	1.7	5.0	13.0	71.6
$Pt/BaO/SiO_2$[a]	2.6	0	0	0	3.9	12.0	84.1
$Pt\text{-}3MgO/SiO_2$-co	13.9	2.0	22.6	13.6	10.9	42.7	8.2
Pt/SiO_2 + MgO	26.5	0	0	3.1	5.9	42.2	48.8

Note: Reaction conditions: T = 400 °C, P = 1.0 MPa, τ = 0.16 min.
[a] $Pt/MO/SiO_2$ (M = Ca, Sr, Ba) refer to the equal mole of alkaline earth metal oxides with that of $Pt/3MgO/SiO_2$.

Table 5
DBF conversion over the Pt/SiO_2 catalysts with alkaline earth metal oxides at equal moles and properties of dopants.

Dopants	Conversion[a] (%)	Metal-Oxygen bond strength[b] (eV)	Metal ionic radius[c] (nm)	Charge/surface[d]
MgO	96	4.3	0.065	1.31
CaO	37	3.6	0.099	1.00
SrO	25	3.3	0.113	0.95
BaO	10	3.0	0.135	0.89

[a] The conversion over Pt/SiO_2 catalyst modified by dopants at τ = 0.36 min.
[b] The data refer as [29].
[c,d] The data refers as lange's handbook of chemistry.

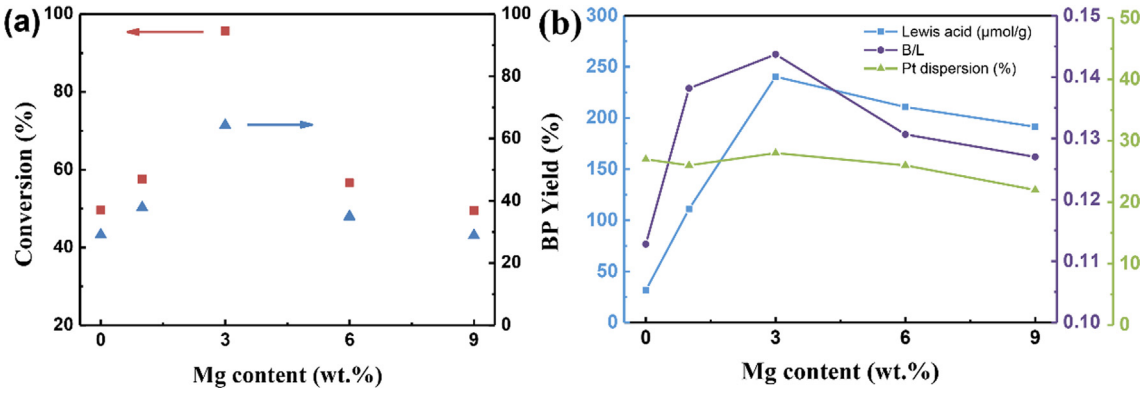

Fig. 6. (a) Influence of the Mg content on the reaction activity and BP yield during the hydrogenolysis of DBF over the $Pt/xMgO/SiO_2$ catalysts (Data refer to 0.36 min of contact time). (b) Effect of the Mg content on the catalysts or supports.

supports. Based on the results of acid-base properties of supports and electronic density of the corresponding catalysts, the different electron density of active component and support acid-base properties originating from the dissimilarity of additive amount of Mg, change the way reactants adsorbed and desorbed on the surface of the catalysts, and thus contribute to the disparity of selectivity [31,49]. The new acidic sites could be created by addition of MgO, which serve as active sites to adsorb the oxygen atom of DBF. However, the desorption of the formed BP without oxygen atom, due to π electrons of aromatic ring acting as a Lewis base, could be promoted by the increased electronic density.

In the hydrogenolysis of DBF, under the same reaction conditions, the negligible difference in the Pt dispersions between the promoted catalysts with various Mg loadings indicates that the structural effect of the MgO on the SiO_2 does not significantly affect the energetic state of the active sites. Nevertheless, the significant differences in activity point out to a significant promoter effect, which must then be contributed to electronic effect. The electron-rich character of Pt sites regularly changed in volcano-type with the MgO addition, is consistent with the volcano-type activities. It indicates that a relationship is established between the changes of electronic properties and the catalytic activity on $Pt/xMgO/SiO_2$ catalysts. The electron transfers from support to Pt nanoparticles accelerate high activity of DBF conversion, and that is in agreement with the previous reports [15,30,38,50]. In particular, Regalbuto et al. [50] studied the effects of alkaline metal promoters on Ru/Al_2O_3 catalysts for hydrogenation of levulinic acid and found that a similar volcano trend, where catalysts promoted with 3 wt% K and 3 wt% Cs exhibited the highest activity in their respective series, is due to the balance between the enhanced electronic density from alkaline metal to Ru and ruthenium site blockage.

Enhanced activity may also involve the promoted hydrogen-spillover effect by Lewis acidic sites of the support, and then facilitated hydrogen activation/dissociation of Pt [13], which corresponds well with the amount of acidic sites in $xMgO/SiO_2$ supports. Previously, it was pointed out that hydrogen spillover onto these non-reducible oxides such as SiO_2, Al_2O_3 and zeolite would be energetically improbable if there are no defect sites that can stabilize atomic hydrogen [51]. However, the modification

with MgO could expose more defects in the SiO_2 support [52], as it can be confirmed by the changes of acid-base properties. Furthermore, the reduction level of active metals is relative to the extent of hydrogen-spillover, the higher hydrogen spillover effect favors the reduction of oxide metals [53]. It was also reported that spillover has been proposed as an explanation for the promotional effect of basic metal oxides on the methanol activity of Pd/SiO_2 [54]. However, H atoms do not reduce the basic metal oxides, and it would be a disadvantage for H atoms to leave the metal surface [51]. One expected that the acidic sites formed by Si—O—Mg bond could promote hydrogen spillover and the excess MgO could block accessibility for hydrogen spillover to the support. Accordingly, the hydrogen adsorption and activation on MgO may happen, but would not be very strong or fast [15], compared with dissociation of molecular hydrogen on active Pt.

Another important factor affecting the activity may be the metal-support interfaces. The interface between the metal particle and the metal-oxide particle may be the area where most of the H atoms react with DBF, formed by the formation of OPP on the interface, to BP. H atoms do not travel much further than the immediate interface between the metal particle and the metal-oxide particle [51]. Moreover, Pt-magnesia-silica interfaces provide a chance for Si—O—Mg bond to improve the hydrogen spillover. On the other hand, the Si—O—Mg chemical bond formed by MgO addition could be necessary for the balanced acid-base sites on the surface in relation to the interaction between MgO and SiO_2 and the consequent high catalytic performance [17]. However, with too much addition of MgO, the access of reactants to Pt surface and interfaces are blocked seriously [55].

3.6.2. Synergistic effect of catalyst on the hydrogenolysis of DBF

The preparation of catalysts has been regarded to be of pivotal importance for catalytic performance. The experimental results (Fig. 7) showed that a physical mixture of Pt/SiO_2 and MgO performed worse than the $Pt/3MgO/SiO_2$ catalyst, even worse than the Pt/SiO_2 catalyst with no MgO, highlighting the synergistic effect that was achieved, and probably the existence of Pt-magnesia-silica interfaces as also confirmed by HRTEM. A last consideration related to the nature of synergistic effect observed for the $Pt/xMgO/SiO_2$ catalysts in the hydrogenolysis of DBF has to do with the method of adding MgO. The activity of the catalyst prepared by sequential impregnation is significantly higher than that of the catalyst prepared by co-impregnation with a similar Mg loading of 3 wt%. That result may be related to the difference of electron density of Pt nanoparticles (Table 3). According to the results of experiment, the method of sequential impregnation could enhance the acid-base properties of SiO_2 and thus increase the electron density of active sites for the hydrogenolysis reactions.

3.6.3. Comparison of alkaline earth metal oxides at equal moles

Based on these findings, we selected the optimal Mg moles of $Pt/3MgO/SiO_2$ catalyst (atomic ratio of Mg/Pt is approximately 50:1) together in use with other alkaline earth metals (Ca, Sr and Ba) in the hydrogenolysis of DBF and the results are plotted in Fig. 8a. Apparently, activity decreased in the order: Mg > Ca > Sr > Ba, which may be due to the difference in Pt dispersions (Table 1), suggesting various dopants reduced the concentration of surface Pt sites responsible for the catalytic reaction by site blocking or masking [56] due to lower surface area. Other explanation could be that it correlates with the decrease in dopant electronegativity (strong basic character) and metal-oxygen bond strength, and the increase of the ionic radius. Most importantly, the conversion of DBF hydrogenolysis increased with increasing the electronegativity (decreasing basic character) of the corresponding alkaline earth metal oxide (Fig. 8b). Differences in the electronegativity values are reflected in the acid-base properties [21] and electronic states, and then contribute to the diverse activities, which proves that stronger basic sites are detrimental to the activity for catalysts. That also was testified by the fact that adding MgO to Pt/SiO_2 (physical mixture) could decrease the activity of Pt/SiO_2. Prins et al. [54] found a volcano curve of reaction rate and the metal ion electronegativity in exploring the promotional effect of basic metal oxides on the silica-supported Pd catalysts in the conversion of synthesis gas to methanol and suggested that the metal oxides with a moderate basic nature were better for CO and CO_2 hydrogenation. Compared with previous results [21,50,54] on the investigation of the relationship between the activities and electronegativity of basic dopants, the reverse trend in this study indicates that acidic sites strongly increase DBF hydrogenolysis, associated with the reaction results over $Pt/xMgO/SiO_2$ catalysts with various acid concentration, and also implies that moderate basic nature may be essential for the high activity and selectivity of catalysts.

3.6.4. Effect of adding 2-methylpiperidine on the hydrogenolysis of DBF over $Pt/3MgO/SiO_2$

In order to probe the effect of acidic sites on the hydrogenolysis of DBF, 2-methylpiperidine was added to the reactant. 2-

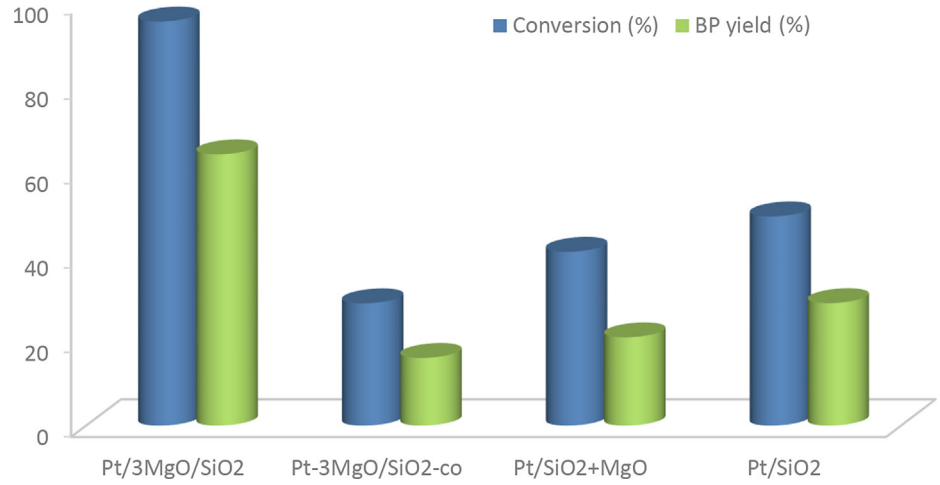

Fig. 7. The conversion of DBF and the yield of BP over $Pt/3MgO/SiO_2$ (sequential impregnation), Pt-$3MgO/SiO_2$-co (co-impregnation), Pt/SiO_2 + MgO (physical mixture), and Pt/SiO_2 catalysts at contact time of 0.36 min.

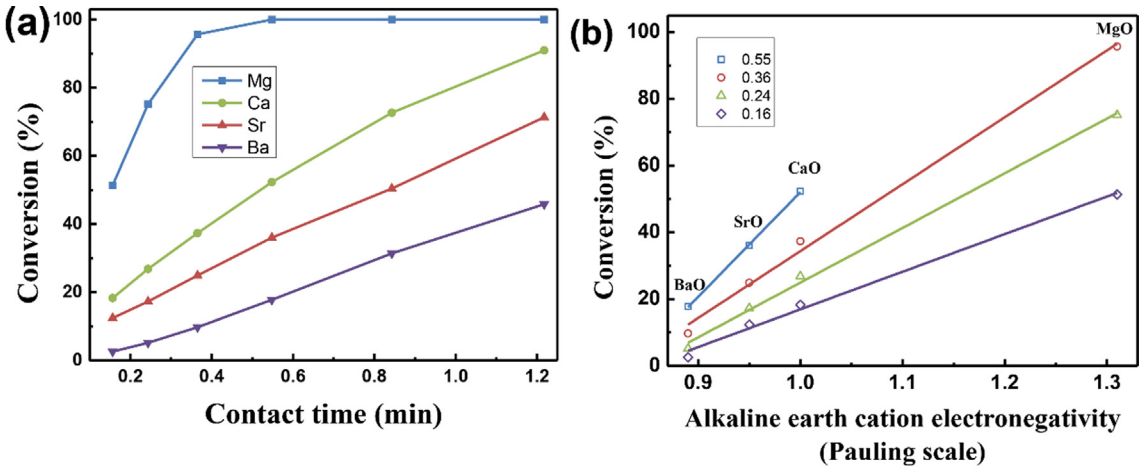

Fig. 8. (a) The effect of the different alkaline earth dopants with equal mole on the conversion of DBF. (b) The conversion of different contact time (min) vs. electronegativity of alkaline earth cation in Pt/MO/SiO_2 (M = Mg, Ca, Sr, Ba) catalysts.

methylpiperidine is considered as a stronger base than pyridine [44], and therefore it might be involved in the preferential adsorption on acidic sites with DBF molecules. The results (Fig. S7) showed that the activity of Pt/3MgO/SiO_2 catalyst for the hydrogenolysis of DBF obviously decreased to 43% from 100% at contact time of 0.55 min and the conversion of 2-methylpiperidine was 100% with the change of contact time. 2-methylpiperidine was found to have strong inhibitory effect, which can be understood on the basis of the competitive adsorption expected due to the strong interaction of this basic molecule with the acidic sites. It is considered that acidic sites as one type of active centers could enhance the hydrogenolysis of DBF.

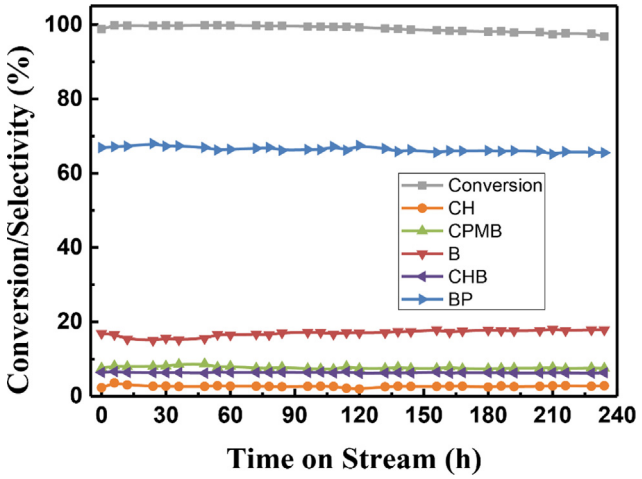

Fig. 9. The time-on-stream results of the long-run test performed over a selected Pt/3MgO/SiO_2 catalyst.

3.7. Stability

To investigate the stability of catalyst at high conversion, time-on-stream analysis on the Pt/3MgO/SiO_2 catalyst was conducted. The DBF conversion and selectivity are displayed in Fig. 9, in which t_0 represents the time when the reactions were stabilized. During the 240 h, the activity and selectivity for Pt/3MgO/SiO_2 catalyst are considerably stable, which could be inferred by the fact that the addition of MgO surrounding Pt may stabilize Pt nanoparticles.

3.8. Reaction mechanism

On the basis of the above results, we formulated a reaction mechanism for the hydrogenolysis of DBF to BP over Pt/xMgO/SiO_2 catalysts, as shown in Fig. 10. For the hydrogenolysis of oxygen-containing hydrocarbons on metal supported catalysts, it is postulated that the reaction occurs at the metal-support interface. The DBF molecule adsorbed on the support is hydrogenated by spilt-over H-species originating from the hydrogen molecule dissociated on the Pt particles [51]. The moderate amount of MgO existed in the metal-support interface accelerates the hydrogenolysis of DBF, mainly, due to the increased Lewis acidic sites and the enhanced electron density of Pt. In the presence of hydrogen, more hydrogen molecules are adsorbed resulting in more active H-species on the catalyst surface due to more active Pt, explaining the increase of DBF conversion in the presence of H_2.

Popov et al. [57] explored the interaction between phenolic compounds and silanol groups present on silica by means of infra-

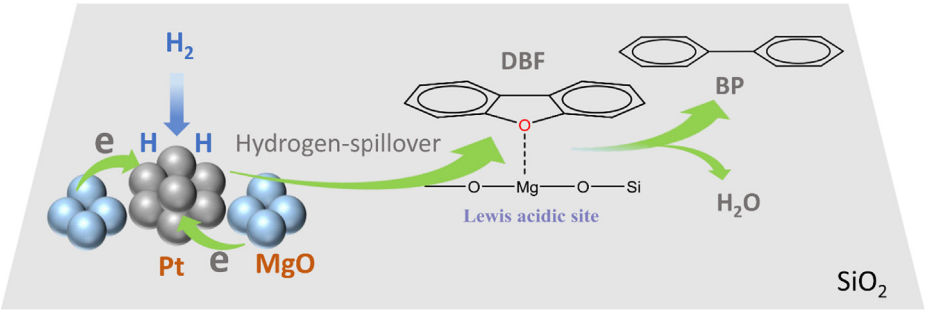

Fig. 10. Supposed schematics of the C-O hydrogenolysis mechanism of DBF over Pt/xMgO/SiO_2 catalysts.

red spectroscopy and found that the silanol protons interact either with the aromatic ring lying coplanarly on the surface or with the oxygenated groups through the oxygen atoms. For DBF molecule, the n-electrons of the oxygen atoms are more basic than the π-electrons of aromatic system. It is considered that the prior adsorption occurs on the Lewis acidic sites of the support by interaction with the oxygen atom rather than with the aromatic ring [58]. Then the cleavage of C-O bond during the hydrogenation of DBF accelerates the formation of OPP and then rapidly produces BP. Besides, the reaction conditions under high temperature and low H_2 pressure maybe also play important roles [5].

4. Conclusions

The relationship between promotional effect of MgO on Pt/SiO_2 and the hydrogenolysis of DBF has been established. Addition of MgO strongly increases the catalytic activity of Pt/SiO_2 catalyst in DBF reaction, which could be associated with an electron enrichment of the Pt surface atoms due to charge transfer as proven by CO-IR and an increase in Lewis acidity as determined by Py-IR and NH_3-TPD. Moreover, comparing the preparation method of catalysts, the activity of the catalyst prepared by sequential impregnation is significantly higher than that of the catalyst prepared by co-impregnation and physical mixture catalyst, indicating electronic effect and metal-support interaction existed and Si—O—Mg bond was formed as also confirmed by IR which could contribute to the changes of acid-base properties. The observed effects of MgO on the selectivity of BP may be interpreted as a combined result of the Lewis acid promoting the adsorption of DBF and the basic property facilitating the desorption of BP. The experimental results of the addition of 2-methylpiperidine to DBF reactant show that the acidic sites could directly accelerate the activity of catalyst by the interaction with oxygen atom in DBF. With the same moles of dopants, the activity of dopants follows the order: Mg > Ca > Sr > Ba, which is attributed to the decrease in Pt dispersion resulting from the structural change and the decrease in electronegativity of alkaline earth metals. Additionally, the addition of MgO effectively stabilizes Pt nanoparticles and the Pt/3MgO/SiO_2 catalyst is stable during the 240 h run.

Acknowledgments

This research was funded by the National Key Research & Development Program of China (2016YFB0600305).

Appendix A. Supplementary material

Supplementary data to this article can be found online at https://doi.org/10.1016/j.jcat.2019.02.017.

References

[1] Y. Wang, T. He, K. Liu, J. Wu, Y. Fang, Bioresour. Technol. 108 (2012) 280–284.
[2] A. Infantes-Molina, E. Moretti, E. Segovia, A. Lenarda, E. Rodríguez-Castellón, Catal. Today 277 (2016) 143–151.
[3] L. Wang, C. Li, S. Jin, W. Li, C. Liang, Catal. Lett. 144 (2014) 809–816.
[4] P. Dong, G.P. Lu, C. Cai, New J. Chem. 40 (2016) 1605–1609.
[5] J.A. Cecilia, A. Infantes-Molina, E. Rodríguez-Castellón, A. Jiménez-López, S.T. Oyama, Appl. Catal., B 136–137 (2013) 140–149.
[6] Y. Wang, Y. Fang, T. He, H. Hu, J. Wu, Catal. Commun. 12 (2011) 1201–1205.
[7] H.W. Lee, B.R. Jun, H. Kim, D.H. Kim, J.K. Jeon, S.H. Park, C.H. Ko, T.W. Kim, Y.K. Park, Energy 81 (2015) 33–40.
[8] A. Infantes-Molina, E. Gralberg, J.A. Cecilia, E. Finocchio, E. Rodríguez-Castellón, Catal, Sci. Technol. 5 (2015) 3403–3415.
[9] J. Zakzeski, P.C.A. Bruijnincx, A.L. Jongerius, B.M. Weckhuysen, Chem. Rev. 110 (2010) 3552–3599.
[10] J. Zhang, L. Wang, C. Li, S. Jin, C. Liang, Org. Process Res. Dev. 22 (2018) 67–76.
[11] C. Liu, Z. Shao, Z. Xiao, C.T. Williams, C. Liang, Energy Fuels 26 (2012) 4205–4211.
[12] I. Graça, D. Iruretagoyena, D. Chadwick, Appl. Catal. B 206 (2017) 434–443.
[13] Y. Liu, J. Zhao, Y. He, J. Feng, T. Wu, D. Li, J. Catal. 348 (2017) 135–145.
[14] K.A. Nadeina, O.V. Klimov, I.G. Danilova, V.Y. Pereyma, E.Y. Gerasimov, I.P. Prosvirin, A.S. Noskov, Appl. Catal. B 223 (2018) 22–35.
[15] W. Chen, H. Nie, D. Li, X. Long, J. van Gestel, F. Maugé, J. Catal. 344 (2016) 420–433.
[16] S.H. Chung, C. Angelici, S.O.M. Hinterding, M. Weingarth, M. Baldus, K. Houben, B.M. Weckhuysen, P.C.A. Bruijnincx, ACS Catal. 6 (2016) 4034–4045.
[17] X. Huang, Y. Men, J. Wang, W. An, Y. Wang, Catal. Sci. Technol. 7 (2017) 168–180.
[18] S. Da Ros, M.D. Jones, D. Mattia, J.C. Pinto, M. Schwaab, F.B. Noronha, S.A. Kondrat, T.C. Clarke, S.H. Taylor, ChemCatChem 8 (2016) 2376–2386.
[19] B. Puértolas, T.C. Keller, S. Mitchell, J. Pérez-Ramírez, Appl. Catal. B 184 (2016) 77–86.
[20] S.W. Lee, S.K. Ihm, Ind. Eng. Chem. Res. 52 (2013) 15359–15365.
[21] D. Prieto-Centurion, A.M. Boston, J.M. Notestein, J. Catal. 296 (2012) 77–85.
[22] B.M. Mogudi, P. Ncube, N. Bingwa, N. Mawila, S. Mathebula, R. Meijboom, Appl. Catal. B 218 (2017) 240–248.
[23] F. Balas, M. Rodríguez-Delgado, C. Otero-Arean, F. Conde, E. Matesanz, L. Esquivias, J. Ramírez-Castellanos, J. Gonzalez-Calbet, M. Vallet-Regí, Solid State Sci. 9 (2007) 351–356.
[24] Y.Y. Li, K.K. Han, W.G. Lin, M.M. Wan, Y. Wang, J.H. Zhu, J. Mater. Chem. A 1 (2013) 12919.
[25] Z. Buniazet, J. Couble, D. Bianchi, M. Rivallan, A. Cabiac, S. Maury, S. Loridant, J. Catal. 348 (2017) 125–134.
[26] Y.H. Xie, B. Li, W.Z. Weng, Y.P. Zheng, K.T. Zhu, N.W. Zhang, C.J. Huang, H.L. Wan, Appl. Catal. A 504 (2015) 179–186.
[27] O. Isaienko, E. Borguet, Langmuir 29 (2013) 7885–7895.
[28] V.K. Diez, C.R. Apesteguia, J.I. Di Cosimo, Catal. Today 63 (2000) 53–62.
[29] H. Idriss, M.A. Barteau, Adv. Catal. 45 (2000) 261–331.
[30] A. Siani, O.S. Alexeev, G. Lafaye, M.D. Amiridis, J. Catal. 266 (2009) 26–38.
[31] F. Hoxha, B. Schimmoeller, Z. Cakl, A. Urakawa, T. Mallat, S.E. Pratsinis, A. Baiker, J. Catal. 271 (2010) 115–124.
[32] B. Schimmoeller, F. Hoxha, T. Mallat, F. Krumeich, S.E. Pratsinis, A. Baiker, Appl. Catal. A 374 (2010) 48–57.
[33] E. Schmidt, W. Kleist, F. Krumeich, T. Mallat, A. Baiker, Chem. Eur. J. 16 (2010) 2181–2192.
[34] D.C. Koningsberger, D.E. Ramaker, J.T. Miller, J. de Graaf, B.L. Mojet, Top. Catal. 15 (2001) 35–42.
[35] G. Blyholder, J. Phy. Chem. 68 (1964) 2772–2777.
[36] R.V. Hardeveld, F. Hartog, Adv. Catal. 22 (1972) 75–113.
[37] F. Stoop, F.J.C.M. Toolenaar, V. Ponec, J. Catal. 73 (1982) 50–56.
[38] T. Visser, T.A. Nijhuis, A.M.J. van der Eerden, K. Jenken, Y. Ji, W. Bras, S. Nikitenko, Y. Ikeda, M. Lepage, B.M. Weckhuysen, J. Phys. Chem. B 109 (2005) 3822–3831.
[39] M. Lepage, T. Visser, A.M.J. van der Eerden, F. Soulimani, B.M. Weckhuysen, Vib. Spectrosc. 48 (2008) 92–100.
[40] M.F.K. Yokota, T. Tanaka, Appl. Surf. Sci. 121 (122) (1997) 273–277.
[41] Y.V. Larichev, J. Phy. Chem. C 115 (2011) 631–635.
[42] S. Dominguez-Dominguez, A. Berenguer-Murcia, D. Cazorla-Amoros, A. Linares-Solano, J. Catal. 243 (2006) 74–81.
[43] S. Dominguez-Dominguez, A. Berenguer-Murcia, A. Linares-Solano, D. Cazorla-Amoros, J. Catal. 257 (2008) 87–95.
[44] J. Zhao, H. Chen, J. Xu, J. Shen, J. Phys. Chem. C 117 (2013) 10573–10580.
[45] S.B.D. Mey, C. Canaff, F. Maugé, C. Bouchy, F. Diehl, J. Catal. 227 (2004) 436–447.
[46] Y. He, J. Fan, J. Feng, C. Luo, P. Yang, D. Li, J. Catal. 331 (2015) 118–127.
[47] C.R. Lee, J.S. Yoon, Y.W. Suh, J.W. Choi, J.M. Ha, D.J. Suh, Y.K. Park, Catal. Commun. 17 (2012) 54–58.
[48] L. Wang, H. Wan, S. Jin, X. Chen, C. Li, C. Liang, Catal. Sci. Technol. 5 (2015) 465–474.
[49] E. Kim, E.W. Shin, C.W. Bark, I. Chang, W.J. Yoon, W.J. Kim, Appl. Catal. A 471 (2014) 80–83.
[50] S. Cao, J.R. Monnier, J.R. Regalbuto, J. Catal. 347 (2017) 72–78.
[51] R. Prins, Chem. Rev. 112 (2012) 2714–2738.
[52] M.A. Aramendia, J.A. Benitez, V. Borau, C. Jimenez, J.M. Marinas, J.R. Ruiz, F. Urbano, Langmuir 15 (1999) 1192–1197.
[53] J. Schumann, M. Eichelbaum, T. Lunkenbein, N. Thomas, M.C. Álvarez Galván, R. Schlögl, M. Behrens, ACS Catal. 5 (2015) 3260–3270.
[54] A. Gotti, R. Prins, J. Catal. 175 (1998) 302–311.
[55] X. Yang, X. Su, X. Chen, H. Duan, B. Liang, Q. Liu, X. Liu, Y. Ren, Y. Huang, T. Zhang, Appl. Catal. B 216 (2017) 95–105.
[56] J. García-Aguilar, D. Cazorla-Amorós, Á. Berenguer-Murcia, Appl. Catal. A 538 (2017) 139–147.
[57] A. Popov, E. Kondratieva, J.M. Goupil, L. Mariey, P. Bazin, J. Gilson, A. Travert, F. Mauge, J. Phy. Chem. C 114 (2010) 15661–15670.
[58] R.N. Olcese, M. Bettahar, D. Petitjean, B. Malaman, F. Giovanella, A. Dufour, Appl. Catal. B 115–116 (2012) 63–73.